# COMPARISON OF SMOOTH- AND ROUGH-WALL NON-EQUILIBRIUM BOUNDARY LAYERS WITH FAVORABLE AND ADVERSE PRESSURE GRADIENTS

**Ralph J. Volino**
Department of Mechanical Engineering
United States Naval Academy
590 Holloway Rd.
Annapolis, Maryland, 21402, USA
volino@usna.edu

**Michael P. Schultz**
Department of Naval Architecture and Ocean Engr.
United States Naval Academy
590 Holloway Rd.
Annapolis, Maryland, 21402, USA
mschultz@usna.edu

## ABSTRACT

Measurements were made in rough-wall boundary layers subject to favorable, zero, and adverse pressure gradients. Profiles of mean velocity and turbulence quantities were acquired, and comparisons were made to equivalent smooth-wall cases with the same freestream velocity distributions. Outer layer similarity was observed between the rough- and smooth-wall cases in all quantities in the favorable and zero pressure gradient regions, but large differences were observed with adverse pressure gradients. The results suggest that similarity might be achieved if cases with the same Clauser pressure gradient parameter history were compared. The results also suggest that the equivalent sandgrain roughness may remain constant for a surface as the pressure gradient is varied.

## INTRODUCTION

Both smooth- and rough-wall boundary layers have been studied extensively under canonical zero pressure gradient (ZPG) conditions, as documented in review articles such as Chung et al. (2021). Roughness increases the drag on the wall, expressed as the skin friction coefficient, $C_f$, or the friction velocity, $u_\tau$, due to the form drag on the roughness elements. The effect of the roughness can be quantified as the roughness function, $\Delta U^+$, which is the shift downward of the mean velocity profile in inner coordinates below the canonical law of the wall, $u^+=(1/\kappa)\ln(y^+)+A$. For a fully rough surface, the roughness function is directly related to the equivalent sandgrain roughness, $k_s$, of the surface by the function $\Delta U^+=(1/\kappa)\ln(k_s^+)+A-8.5$, based on the work of Nikuradse (1933). Although $k_s$ is a hydrodynamic quantity (a function of the increase in $u_\tau$ compared to the smooth wall, not a physical dimension of the surface), it has been observed under ZPG conditions to remain approximately constant for a given physical roughness. Predicting $k_s$ from the physical roughness geometry has been the subject of considerable research as discussed in Flack and Chung (2022). Once $k_s$ is obtained for a given rough surface, it can be used for computational predictions at any Reynolds number as long as fully rough conditions are met (typically taken as $k_s^+>80$).

In the outer region of the boundary layer, Townsend (1976) proposed similarity between rough- and smooth-wall boundary layers when scaled with the boundary layer thickness, $\delta$, and $u_\tau$. Similarity implies that the structure in the outer part of the boundary layer is the same in rough- and smooth-wall cases, with the wall shear serving only as a boundary condition. Some exceptions to similarity have been observed, such as when the roughness height is a large fraction of $\delta$, but in general, outer similarity has been shown to be very robust in ZPG boundary layers.

Many boundary layers of practical interest occur under approximately ZPG conditions. An example is the boundary layer on the side of a large ship. In many other cases of interest, however, significant non-zero pressure gradients are present. Examples include the flows around airfoils and planing surfaces on naval vessels, and in many cases the surfaces in question are rough. Although some notable studies of the combined effects of roughness and pressure gradients can be found in the literature, there has been considerably less work than in the more canonical cases. Important questions remain to be answered. Does $k_s$ for a surface remain constant in the presence of a pressure gradient? Is outer layer similarity between rough- and smooth-wall cases preserved, and if so, what flow parameters result in similarity?

The present study investigates rough-wall boundary layers with non-equilibrium pressure gradients under a range of Reynolds number and acceleration parameters, $K=\nu/U_\infty^2(dU_\infty/dx)$, where $\nu$ is the kinematic viscosity, $x$ is the streamwise coordinate, and $U_\infty$ is the local freestream velocity. Experiments were done in the same facility and under the same conditions as the smooth-wall study of Volino (2020). The present paper focuses on mean velocity and turbulence statistics, and the extent of similarity with the smooth-wall results.

## EXPERIMENTS

Experiments were conducted in the water tunnel described in Volino (2020). The test section, shown schematically in Fig. 1, was 2 m long, 0.2 m wide, and 0.1 m tall at the inlet. The lower wall was a flat plate that served as the test wall. The boundary layer was tripped with a 0.8 mm diameter wire at the leading edge. Immediately downstream of the trip the wall was smooth, followed by uniform roughness beginning 0.23 m downstream of the trip. The roughness was random and mathematically generated with the parameters listed in Table 1. This is the same positively skewed roughness used in the ZPG study of Flack et al. (2020). The upper wall was comprised of four flat plates that were independently adjusted. The first section was set to provide a ZPG entry region that extended from the inlet to $x$=0.6 m. The second provided a favorable pressure gradient (FPG) from 0.6 to 1.1 m. The third was set for a ZPG recovery from 1.1 to 1.6 m, and the last section was set for an adverse pressure gradient (APG) from 1.6 to 1.8 m. Cases were considered for three inlet freestream velocities ($U_{\infty o}$=0.5, 1, and 2 m/s), and four positions of the upper wall, including ZPG baseline cases. For the non-ZPG, $K$ in the FPG was equal to $2\times10^{-6}$ (strong ramp), $1\times10^{-6}$ (moderate), and $0.5\times10^{-6}$ (mild) for the $U_{\infty o}$=0.5 m/s cases with the three different upper wall positions, respectively. For the higher
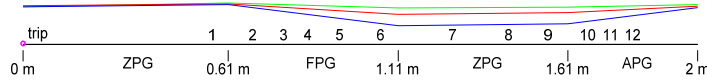
Figure 1. Cross section of test section in streamwise-wall normal plane. Three positions of upper wall shown: blue = strong ramp, red = moderate ramp, green = mild ramp. Numbers 1-12 indicate streamwise measurement stations.

Table 1. Rough surface statistics.

| $k_a$ (μm) | $k_{rms}$ (μm) | $k_t$ (mm) | $k_s$ (mm) | $Sk$ | $Ku$ | $ES$ |
| --- | --- | --- | --- | --- | --- | --- |
| 277 | 350 | 3.5 | 2.2 | 0.98 | 4.18 | 0.4 |

inlet velocities at each position, $K$ was inversely proportional to $U_{\infty o}$. Constant, positive $K$ flows approach equilibrium on a smooth wall. In the APG region, $K$ was constant with a value opposite in sign and half the magnitude of $K$ in the upstream FPG for each case. Equilibrium in APG flows requires a constant Clauser pressure gradient parameter, $\beta=KRe_{\delta*}/(C_f/2)$, where $Re_{\delta*}$ is the displacement thickness Reynolds number. The $\beta$ value continuously rose in the APG regions of the present study, so they were not in or approaching equilibrium.

Velocity profiles were acquired along the spanwise centerline of the test section at the 12 streamwise stations shown in Fig. 1. The profiles were measured with a TSI FSA3500 two-component laser-Doppler velocimeter (LDV). The LDV included a four-beam fiber optic probe with a custom beam displacer that was used to shift one of the beams, resulting in three co-planar beams that were aligned parallel to the wall. A 2.6:1 beam expander was located at the exit of the probe to reduce the diameter of the measurement volume to 45 μm. The probe volume length was 340 μm. The flow was seeded with 2 μm diameter silver-coated glass spheres. Data were acquired in coincidence mode. Each profile included 43 locations extending from the roughness surface to the freestream. Data were acquired at each location for 10,000 large eddy turnover times ($\delta/U_\infty$).

**RESULTS**

Under fully rough, ZPG conditions, boundary layers are invariant with freestream velocity (i.e., $C_f$, and the boundary layer thicknesses remain constant at a given streamwise location), as explained in Pullin et al. (2017), and this was also observed in the present non-ZPG cases. Results are shown below for the $U_{\infty o}$=1 m/s cases.

Figure 2 shows mean streamwise velocity profiles in defect coordinates for the strong ramp configuration. The method of Volino and Schultz (2018), which utilizes the measured Reynolds shear stress and mean velocity profiles, was used to determine $u_\tau$ for each profile. In Fig. 2, the present rough-wall data are shown with symbols, and the corresponding smooth-wall data of Volino (2020) are shown with lines. The profiles are depressed toward a new equilibrium by the FPG (Fig. 2a). The progress toward the new equilibrium appears to be slightly faster for the rough wall, but the smooth- and rough-wall cases are otherwise quite similar. In the ZPG recovery (Fig. 2b), the smooth and rough cases both go back to similar canonical ZPG conditions, with the rough wall cases appearing to proceed somewhat more rapidly to the new condition. Devenport and Lowe (2022) show that the length scale for adjustment to a change in pressure gradient is $2\theta/(C_f\beta)=\nu/(HU_\infty K)$, where $\theta$ is the momentum thickness and $H=\delta^*/\theta$ is the shape factor. For the smooth- and rough-wall cases of Fig. 2, $\nu$, $U_\infty$, and $K$ are the same, and $H$ is about 20% higher in the rough wall case.

This suggests that the adjustment to the pressure gradient should be somewhat more rapid in the rough-wall case. The roughness has a strong effect on the boundary layer, with $\delta$ and $u_\tau$ increased by about 30% and 50% respectively above the smooth wall values in the ZPG and FPG, but in defect coordinates, outer region similarity is still apparent. In the APG (Fig. 2c), the behavior changes. The profiles are much less full in the rough-wall case, and the dimensionless velocities are much higher.

A potentially important difference between the rough and smooth cases in the APG is that $\beta$ was much higher for the rough wall, increasing from 6.5 to 73 between stations 10 and 12 with the rough wall and from 2.7 to 6.6 with the smooth wall. Figure 3 shows the mean velocity profiles from the moderate ramp case (symbols) and the smooth-wall results from the strong ramp case (solid lines) and the moderate ramp case (dashed lines). In the FPG and ZPG recovery regions, the rough-wall results are similar to the corresponding moderate ramp smooth-wall profiles, in agreement with the results of Fig. 2. The profiles do not deviate as much from ZPG conditions as those with the strong ramp. In the APG, the rough-wall results fall between those of the moderate and strong ramp. The $\beta$ values were 1.3-1.9, 0.79-1.02, and 2.7-6.6, for the rough, moderate ramp smooth, and strong ramp smooth cases, respectively. These results suggest that if the $\beta$ history were the same for rough- and smooth-wall cases, that outer region similarity might hold.

The Reynolds stresses and higher order moments were examined, and the same similarity between the rough- and smooth-wall cases was observed for all quantities. The streamwise component of the Reynolds stress, $u'^2$, is shown in Fig. 4 for the strong ramp cases in the same format as Fig. 2. As expected, the near wall peak of the smooth wall profiles, which occurs in the buffer region, is not present in the rough wall cases. The near wall peak is due primarily to viscous effects near the wall, and this region is disrupted by the roughness elements, with the viscous drag replaced by pressure drag on the roughness. In the outer region, there is similarity between the smooth- and rough-wall cases in the initial ZPG region. As with the mean velocity profiles, this similarity largely holds through the FPG and ZPG recovery regions, but the rough-wall cases appear to respond more quickly to the changes in pressure gradient and reach their new equilibrium faster. In the APG region, the similarity is lost. The boundary layer grows and approaches separation faster on the rough wall, resulting in a more rapid drop in $u_\tau$. The result is $u'^2/u_\tau^2$ an order of magnitude larger in the rough wall case by the last station in the APG.

Figure 5 shows $u'^2$ for the moderate ramp rough-wall case with comparison to the smooth wall cases in the format of Fig. 3. In the FPG, the moderate ramp results in less change in the profiles than in the strong ramp case of Fig. 4. The trend is the same however, with the acceleration suppressing the turbulence in the outer region, agreement with the corresponding, moderate ramp, smooth-wall case, and more rapid change toward a new equilibrium with the rough wall. The behavior in the ZPG recovery is the same. In the APG region, the rough-wall and moderate ramp smooth-wall profiles do not agree,

2
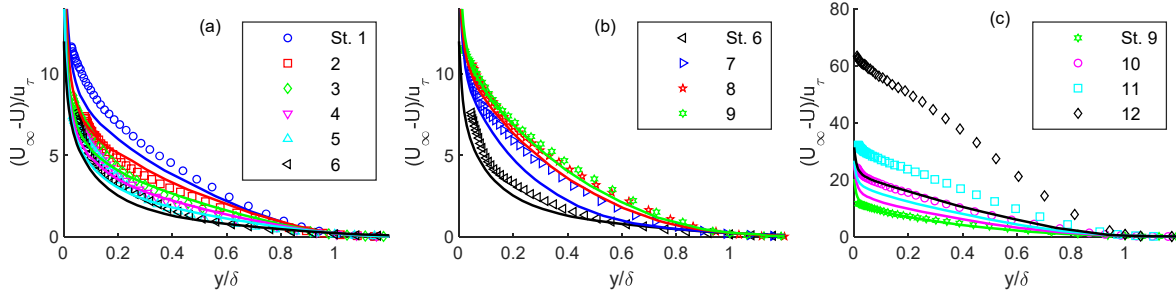
Figure 2. Mean velocity profiles in defect coordinates, a) FPG, b) ZPG recovery, c) APG. Strong ramp case. Symbols – rough wall, lines – smooth wall. Symbol and line color match at each station.
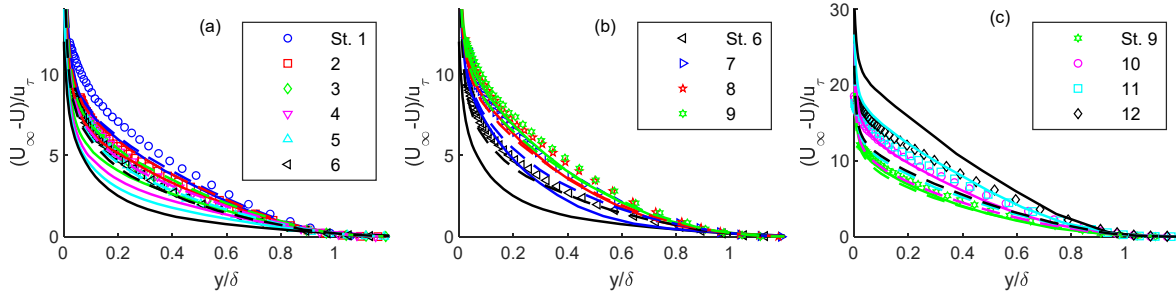


Figure 3. Mean velocity profiles in defect coordinates, a) FPG, b) ZPG recovery, c) APG. Symbols – rough wall w/ moderate ramp, solid lines – smooth wall with strong ramp, dashed lines – smooth wall with moderate ramp.
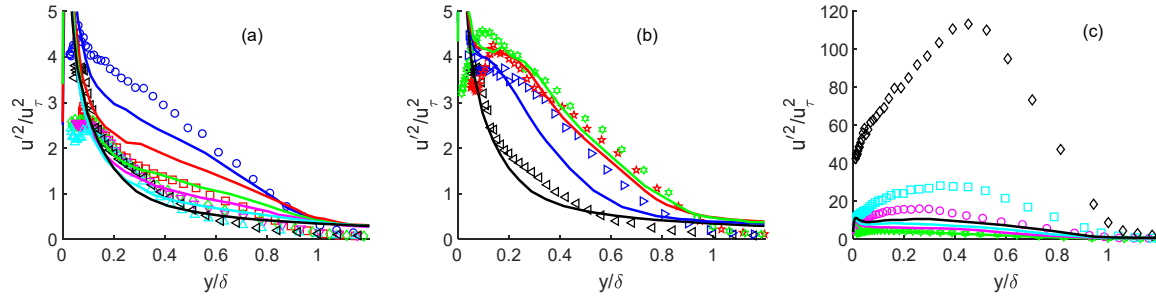


Figure 4. Streamwise component of Reynolds normal stress profiles, a) FPG, b) ZPG recovery, c) APG. Strong ramp case. Same legend as Fig. 2.
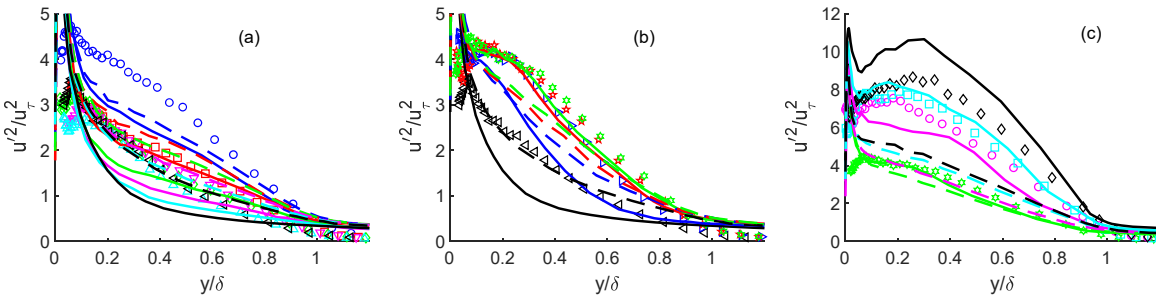


Figure 5. Streamwise component of Reynolds normal stress profiles, a) FPG, b) ZPG recovery, c) APG. Symbols – rough wall w/ moderate ramp, solid lines – smooth wall with strong ramp, dashed lines – smooth wall with moderate ramp. Same legend as Fig. 3.

with the values in the rough wall case approaching double those of the smooth-wall by the end of the APG. As with the mean profiles of Fig. 3, there is better agreement between the moderate ramp rough-wall profiles and the strong ramp smooth-wall profiles.

Reynolds shear stress, $-u'v'$, profiles are shown in Figs. 6 and 7 in the same format as Figs. 4 and 5. As with the mean velocity and $u'^2$, similarity between the rough- and smooth-wall cases with the same $K$ is seen in the FPG and ZPG recovery for both the strong and moderate ramp cases, with the rough wall

3
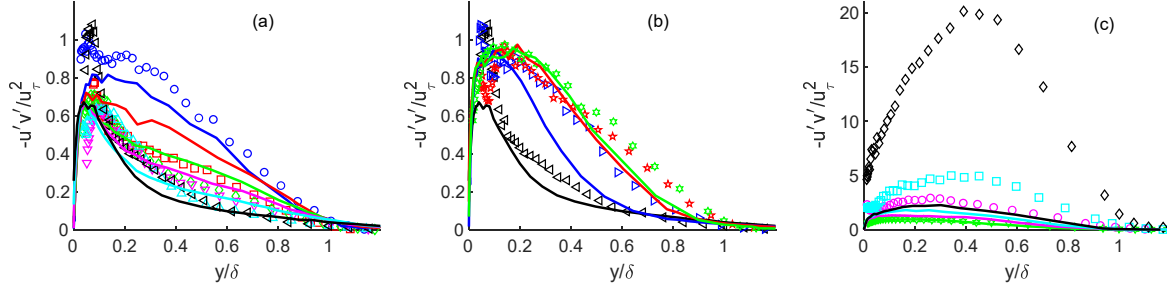
Figure 6. Reynolds shear stress profiles, a) FPG, b) ZPG recovery, c) APG. Strong ramp case. Same legend as Fig. 2.
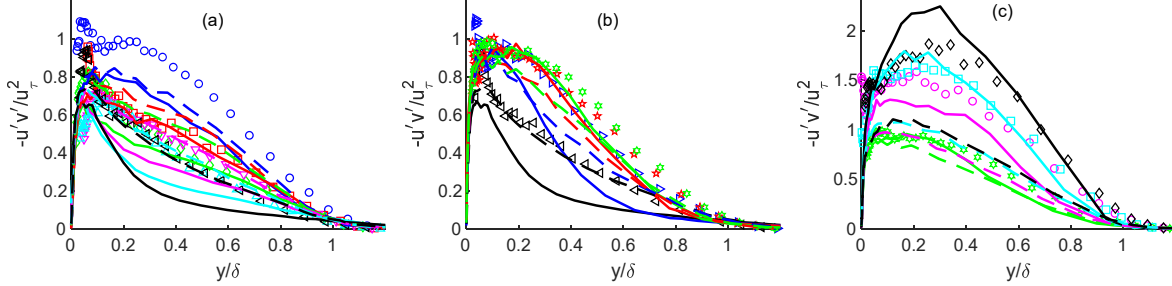


Figure 7. Reynolds shear stress profiles, a) FPG, b) ZPG recovery, c) APG. Symbols – rough wall w/ moderate ramp, solid lines – smooth wall with strong ramp, dashed lines – smooth wall with moderate ramp. Same legend as Fig. 3.

cases proceeding somewhat more rapidly to the new equilibrium. In the APG region, as with the quantities presented above, the best agreement is between cases with different velocity distributions but more similar $\beta$ histories.

The behavior observed in the Reynolds stresses is also present in the higher order moments. Profiles of $u'^2v'$, are shown in Figs. 8 and 9 as an example. In the FPG and ZPG regions, there is similarity between the rough- and smooth-wall cases with the same freestream velocity distribution. In the APG flow, the rough- and smooth-wall cases again show better agreement when cases with more similar $\beta$ histories are compared.

Another way of evaluating similarity or differences between cases is with the diagnostic plot, which was applied to rough wall boundary layers by Castro et al. (2013). Profile data for rms $u'$ is normalized by the local mean velocity $U$, and plotted vs the local $U$ normalized by $U_\infty$. An example is shown for the FPG and ZPG recovery region profiles of the moderate ramp smooth- and rough-wall case in Fig. 10a. The smooth-wall data collapse and lie just above the expected smooth wall line given in Castro et al. (2013) for ZPG cases. The rough-wall profiles collapse onto a different line, which also agrees with ZPG results from Castro et al. (2013). The FPG has no discernable effect on the profiles in these coordinates. To collapse the all data, Castro et al. (2013) introduced modified coordinates, plotting $u'/(U+\Delta U)$ vs $(U+\Delta U)/(U+\Delta U)$, where $\Delta U=u_\tau\Delta U^+$ is a dimensional form of the roughness function. The profiles of Fig. 10a are shown in these coordinates in Fig. 10b, and they collapse onto the smooth wall line, as expected. The profiles from the strong and mild ramp cases (not shown) also collapse onto the same lines.

The diagnostic plots for the APG region profiles are shown in the original coordinates in Fig. 11 and the modified coordinates in Fig. 12. For the weak and moderate ramp cases, there is no significant difference from the ZPG results. In the

strong ramp cases, there is a slight rise in the profiles in the smooth-wall case, and a larger rise in the rough-wall case. It appears that if $\beta$ becomes large enough and the boundary layer begins to approach separation, there is a departure from similarity from the ZPG behavior in the diagnostic plot coordinates.

From the mean profiles, $\Delta U^+$ was determined and is shown as a function of $k_s^+$ for all the cases of the present study in Fig. 13. There is considerable scatter but reasonable agreement with the expected line for the cases with fully rough conditions. In the APG region of the strong ramp cases, $u_\tau$ drops to low values, resulting in transitionally rough behavior with a corresponding drop below the fully rough correlation. In the fully rough cases, there is no obvious trend with pressure gradient. It appears that at least for the cases of the present study, with their particularly pressure gradient histories, that an assumption of a constant $k_s$ with varying pressure gradient may be justified.

The skin friction coefficient is shown in Fig. 14 as a function of $\theta/y_o$ for all the rough and smooth wall cases. These coordinates were shown in Castro (2007) to result in similarity for a large range of rough surfaces. When fully rough, $y_o$ is proportional to $k_s$ and is the $y$ value where the log region of the mean velocity profile in inner coordinates extrapolates to $u^+=0$. The APG data fall below the expected ZPG correlation. Kays and Crawford (1980) suggest an empirical correction to $C_f$ of $(1+\beta/5)$. For the present results, $(1+\beta/6)$ provided a somewhat better fit, and this is shown in Fig. 14b. Kays and Crawford (1980) indicate the correction is applicable for equilibrium flows with constant $\beta$, but it also works well with the present cases. At the most downstream station of the APG in the strong ramp cases, $(1+\beta/6)$ produces an overcorrection. This may be due to the flow being in the transitionally rough regime.
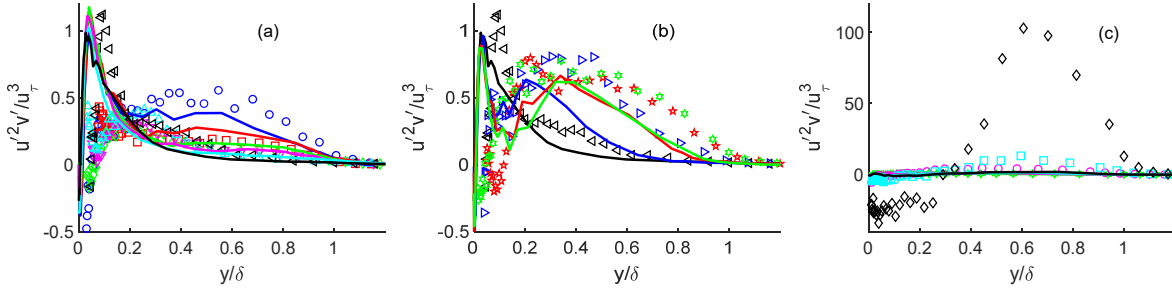
Figure 8. $u'^2v'$ profiles, a) FPG, b) ZPG recovery, c) APG. Strong ramp case. Same legend as Fig. 2.
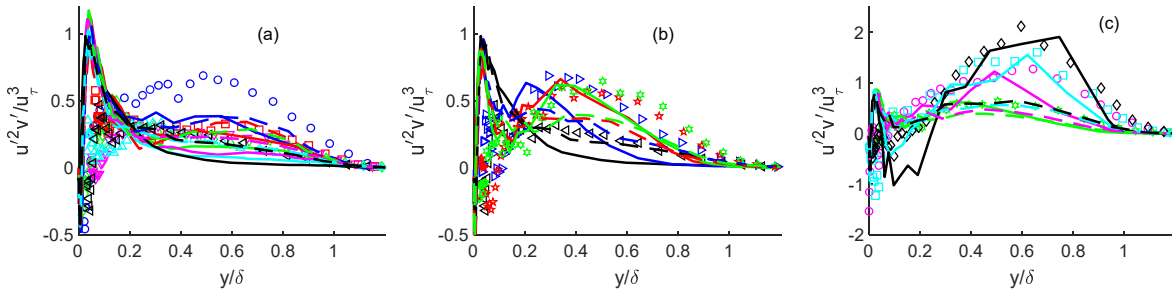


Figure 9. $u'^2v'$ profiles, a) FPG, b) ZPG recovery, c) APG. Symbols – rough wall w/ moderate ramp, solid lines – smooth wall with strong ramp, dashed lines – smooth wall with moderate ramp. Same legend as Fig. 3.
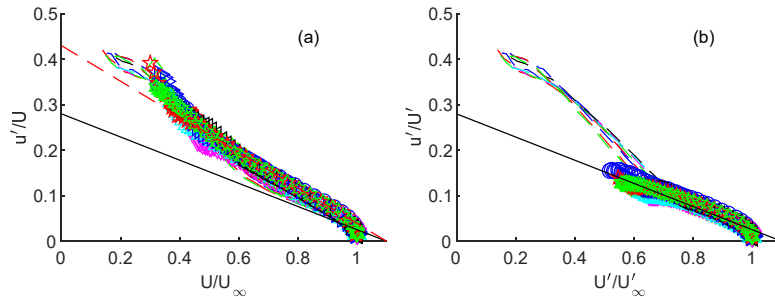


Figure 10. Diagnostic plots for FPG and ZPG profiles of moderate ramp cases, a) standard coordinates, b) modified coordinates. Symbols – rough wall, dashed lines – smooth wall. Same legend as Fig. 2. Straight black line and dashed straight red line are from Castro et al. (2013) for ZPG smooth and rough cases, respectively.
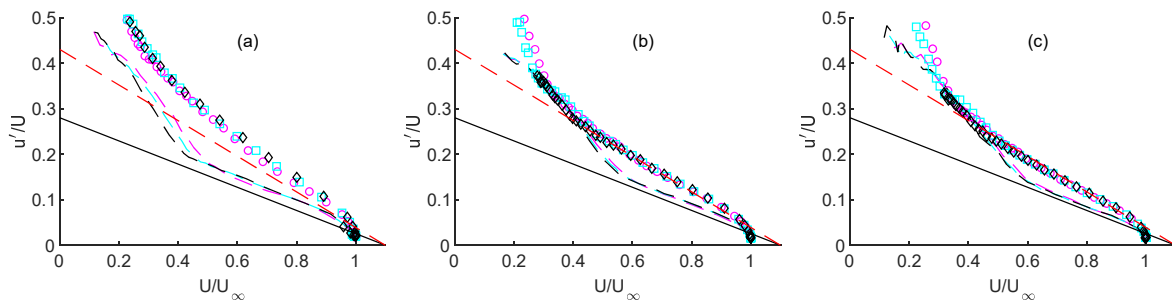


Figure 11. Diagnostic plots for APG profiles in standard coordinates, a) strong ramp, b) moderate ramp, c) mild ramp. Symbols – rough wall, dashed lines – smooth wall. Same legend as Fig. 2. Straight black line and dashed straight red line are from Castro et al. (2013) for ZPG smooth and rough cases, respectively.
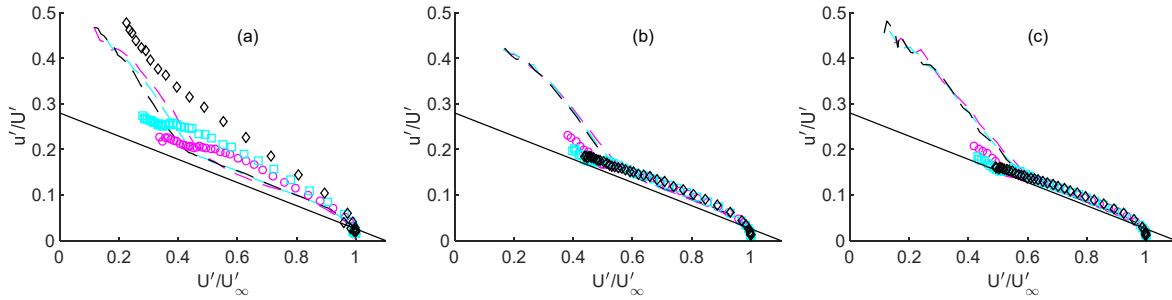
Figure 12. Diagnostic plots for APG profiles in modified coordinates, a) strong ramp, b) moderate ramp, c) mild ramp. Symbols – rough wall, dashed lines – smooth wall. Same legend as Fig. 2. Straight black line from Castro et al. (2013) for ZPG cases.
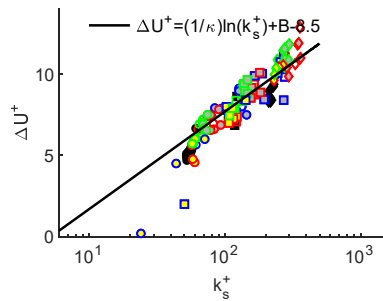


Figure 13. Roughness function as a function of $k_s^+$. Open symbols – ZPG, gray filled – FPG, yellow filled – APG.
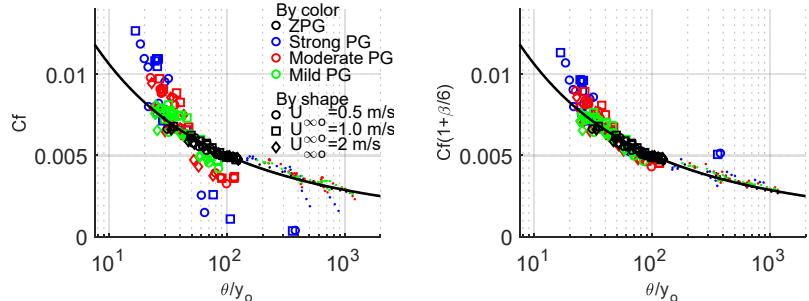
Figure 14. Skin friction coefficient as a function of momentum thickness and roughness length, a) uncorrected, b) corrected with $(1+\beta/6)$. Rough wall – large symbols, smooth wall – small symbols.

## CONCLUSIONS

Mean velocity and turbulence profiles were measured in boundary layers on a rough wall subject to zero, favorable, and adverse pressure gradients. Reynolds numbers and the strength of the pressure gradient were varied. Comparisons were made to smooth-wall cases with the same freestream velocity distributions. The rough-wall results were invariant with Reynolds number, in agreement with previous observations in ZPG flows. In FPG and ZPG regions, the profiles of all quantities showed similarity between the smooth- and rough-wall results, with the rough-wall cases moving somewhat more quickly to a new equilibrium when the pressure gradient was changed. In APG regions, large departures from similarity were observed. This was attributed to the more rapid growth of the rough-wall boundary layer, particularly in the strongest pressure gradient cases. When cases with different dimensional pressure gradients, but more similar $\beta$ histories were compared, the smooth- and rough-wall cases were more similar. Diagnostic plots were also useful for showing the similarity in FPG and ZPG regions, and the departure from similarity with an APG. The results from all cases suggest that the equivalent sandgrain roughness for a surface may remain constant in the presence of a non-zero pressure gradient.

## REFERENCES

Castro, I. P., 2007, "Rough-wall boundary layers: mean flow universality", *Journal of Fluid Mechanics*, Vol. 585, pp. 469-485.

Castro, I. P., Segalini, A., and Alfredsson, P. H., 2013, "Outer-layer turbulence intensities in smooth- and rough-wall boundary layers", *Journal of Fluid Mechanics*, Vol. 727, pp. 119-131.

Chung, D., Hutchins, N., Schultz, M. P., and Flack, K. A., 2021, "Predicting the Drag of Rough Surfaces", *Annual Review of Fluid Mechanics*, Vol. 53, pp. 439-471.

Flack, K., and Chung, D., 2022, "Important Parameters for a Predictive Model of $k_s$ for Zero Pressure Gradient Flows", AIAA 2022-1036, *Proceedings, AIAA SCITECH 2022 Forum*.

Flack, K. A., Schultz, M. P., and Volino, R. J., 2020, "The effect of a systematic change in surface roughness skewness on turbulence and drag", *International Journal of Heat and Fluid Flow*, Vol. 85, 108669.

Devenport, W. J., and Lowe, K. T., 2022, "Equilibrium and non-equilibrium turbulent boundary layers", *Progress in Aerospace Sciences*, Vol. 131, 100807.

Kays, W. M., and Crawford, M. E., 1980, *Convective Heat and Mass Transfer*, 2nd Ed., McGraw-Hill Book Company, New York, p. 189.

Nikuradse, J., 1933, "Laws of flow in rough pipes", *NACA Technical Memorandum 1292* (1950).

Pullin, D. I., Hutchins, N., and Chung, D., 2017, "Turbulent flow over a long flat plate with uniform roughness," *Physical Review Fluids*, Vol. 2, 082601.

Townsend, A. A., 1976, *The Structure of Turbulent Shear Flow*, 2nd Ed., Cambridge University Press, Cambridge.

Volino, R. J., and Schultz, M. P., 2020, "Determination of wall shear stress from mean velocity and Reynolds shear stress profiles", *Physical Review Fluids*, Vol. 3, 034606.

Volino, R. J., 2020, "Non-equilibrium development in turbulent boundary layers with changing pressure gradients", *Journal of Fluid Mechanics*, Vol. 897, A2.